www.springer.com/41230
https://doi.org/10.1007/s41230-026-5182-6

Effect of Nb, Ti introduction sequence on adsorption of Nb on TiB_2 surface and grain refinement performance of Al-4Ti-1Nb-1B

Hao Yi[1, 2], *Ying Cheng[1, 2], **Hua-rui Zhang[1, 2], and Hu Zhang[1, 2]

1. School of Materials Science and Engineering, Beihang University, Beijing 100191, China

2. Ningbo Institute of Technology (NIT), Beihang University, Ningbo 315000, Zhejiang, China

Abstract: In recent years, Al-Ti-Nb-B grain refiners have attracted increasing attention due to their grain refinement performance and anti-Si poisoning ability. This study investigates the influence of the introduction sequence of Ti and Nb during the synthesis of Al-4Ti-1Nb-1B refiners on their refinement performance on CP-Al and a series of Al-Si alloys (Al-3.5Si, Al-7Si, and Al-10.5Si). It is found that Al-4Ti-1Nb-1B prepared by introducing Ti prior to Nb exhibits the best grain refinement and anti-Si poisoning compared to samples where Nb is introduced before Ti or where both are added simultaneously. This Ti-first approach demonstrates superior grain refinement performance across CP-Al, Al-3.5S1, Ai-7Si, and Al-10.5Si alloys, especially at higher Si contents. It refines the grain size of Al-7Si to 150.1±27.5 μm from over 1,500 μm for the unrefined alloy. This superior performance is attributed to the variation in ground-state energy ΔE for the Ti prior to Nb sequence is lower than that of other sequences, thereby facilitating Nb adsorption on the TiB_2 surface. TEM observations corroborate these findings, showing that TiB_2 prepared by this sequence has the highest average Nb content of 3.80at.%. First-principles calculations reveal that this unique Nb adsorption enhances the TiB_2/Al interfacial adhesion energy W_{ad} and suppresses the segregation tendency of Si atoms at the interface, $\kappa_{Si}(c_{Si})$. The higher the Nb adsorption at the TiB_2/Al interface, the stronger the resistance to Si poisoning. These findings underscore the pivotal role of Nb-modified TiB_2 in improving grain refinement and offer a novel strategy for advancing grain refiner technologies in Al-Si alloys.

Keywords: introduction sequence; grain refinement; Nb adsorption; nucleation mechanism

CLC numbers: TG146.23 **Document code:** A **Article ID:** 1672-6421(2026)03-357-10

1 Introduction

Cast Al-Si alloys are widely used in modern industries, such as aerospace, aviation, construction, and transportation, due to their excellent castability, lightweight nature, and corrosion resistance[1-4]. During the casting of Al-Si alloys, grain refinement is a critical process, as it effectively refines primary α-Al grains, thereby improving both the castability and mechanical properties of the alloys[5, 6]. Currently, the most common grain refinement strategy involves the addition of grain refiners into the Al-Si melt[7, 8], among which the Al-5Ti-1B grain refiner is the most extensively used. However, during practical applications, the presence of Si in the Al-Si melt can lead to the formation of silicides, such as $TiSi_2$ and Ti_5Si_3 on the surface of TiB_2 particles in Al-5Ti-1B[9, 10]. These silicides inhibit the heterogeneous nucleation of α-Al, resulting in a significant deterioration of grain refinement performance in Al-Si alloys[11, 12], especially Al-Si alloys with Si content exceeding 5wt.%, which is commonly known as the Si-poisoning effect.

In recent years, novel grain refiners have been developed to overcome the issue of Si-poisoning in Al-Si alloys. Nb has attracted attention due to its ability to form $NbAl_3$ and NbB_2 phases, which are analogous to $TiAl_3$ and TiB_2 in Al-5Ti-1B. Consequently, Al-Nb-B grain refiners are developed and have

*Ying Cheng
Male, born in 1991, Ph. D. His research primarily focuses on melt quality control and solidification microstructure regulation of aluminum alloys.
E-mail: cying@buaa.edu.cn
**Hua-rui Zhang
E-mail: huarui@buaa.edu.cn

Received: 2025-08-05; Revised: 2025-10-04; Accepted: 2025-11-06

demonstrated better grain refinement performance in Al-Si alloys compared to conventional Al-5Ti-1B refiners[13-15]. This improvement is primarily attributed to the higher thermodynamic stability of $NbAl_3$ compared to $TiAl_3$, which makes it less reactive with Si to form Nb-based silicides such as $NbSi_2$, Nb_3Si, and Nb_5Si_3[16-18]. However, the limited anti-fading performance of Al-Nb-B restricts its widespread industrial applications[19, 20]. To address this limitation, researchers have attempted to integrate the advantages of both Ti and Nb, leading to the development of Al-Ti-Nb-B grain refiners. Xu et al.[21] developed an Al-1.67Ti-3.33Nb-0.5B refiner and reported that (Nb, Ti)B_2 particles acted as highly effective heterogeneous nucleation sites for α-Al in Al-Si alloys. Li et al.[22, 23] introduced Ti into the Al-Nb-B melt, forming (Nb, Ti)B_2 core-shell structure with TiB_2 as the core and NbB_2 as the shell, which also exhibited excellent resistance to Si poisoning. Wu et al.[24] synthesized an Al-3.5Nb-1Ti-1B refiner containing (Ti, Nb)B_2 particles with a distinctive sandwich-like Nb-Ti-Nb structure, achieving notable refinement performance in Al-Si alloys. Additionally, Li et al.[25-27] developed the TCB refiner based on the Al-Ti-B-C system, and Xue et al.[28] proposed an Al-4.2V-1.8B refiner. Both refiners demonstrated excellent refinement efficiency in Al-Si alloys and provide valuable insights into overcoming Si poisoning.

Among these recently developed grain refiners, Al-Ti-Nb-B has emerged as a promising and significant candidate. Our previous study[29] observed a nanoscale Nb adsorption layer on the $(01\bar{1}0)$ plane of TiB_2, which can activate TiB_2 as an effective heterogeneous nucleus for α-Al. The composition design and processing parameters significantly influence the morphology and structure of the resulting borides. Ti and Nb are the two most critical refining elements in the Al-Ti-Nb-B system, and the sequence in which they are introduced plays a crucial role in achieving Nb adsorption on the TiB_2 surface, thereby affecting both the grain refinement efficiency and Si-poisoning resistance.

In this study, Al-4Ti-1Nb-1B grain refiners were prepared via different sequences for introducing Ti and Nb to investigate their influence on Nb adsorption at the TiB_2 surface and refinement performance. The grain refinement performance of the prepared refiners were evaluated on CP-Al, Al-3.5Si, Al-7Si, and Al-10.5Si alloys. The Nb adsorption behavior on the TiB_2 surface was quantitatively characterized and compared via transmission electron microscopy (TEM) and energy dispersive spectroscopy (EDS) line-scanning techniques. First-principles calculations were further applied to elucidate the mechanisms underlying Nb atom adsorption and its impact on grain refinement performance and Si-poisoning resistance. These findings provide valuable guidance for the innovative design of Al-Ti-Nb-B grain refiners and contribute to the development of more efficient grain refinement strategies for Al-Si alloys.

2 Experiment method

2.1 Preparation process of Al-4Ti-1Nb-1B master alloys

A series of Al-4Ti-1Nb-1B alloys were synthesized via different Nb and Ti introduction sequences. Al-10Ti and Al-8B master alloys were first put into a SiC crucible at a stoichiometric Ti/B ratio of 2.2 and melted at 800 °C. The melt was stirred and held for 30 min to ensure the complete formation of TiB_2. Subsequently, as illustrated in Fig. 1, Al-10Nb and Al-10Ti were introduced into the melt in three different sequences, followed by an increase in temperature to 900 °C. Figure 1(a) shows the process in which Nb was added prior to Ti; the resulting refiner is labeled as A-Al-4Ti-1Nb-1B (Sample A). In contrast, Fig. 1(b) depicts the process where Ti was added before Nb, producing a refiner designated as B-Al-4Ti-1Nb-1B (Sample B). Figure 1(c) illustrates the simultaneous addition of Ti and Nb, resulting in C-Al-4Ti-1Nb-1B (Sample C). During the holding time, all melts were stirred using a graphite rod at a constant rotation speed. Finally, the melt was poured into a plate-shaped mold preheated to 200 °C.

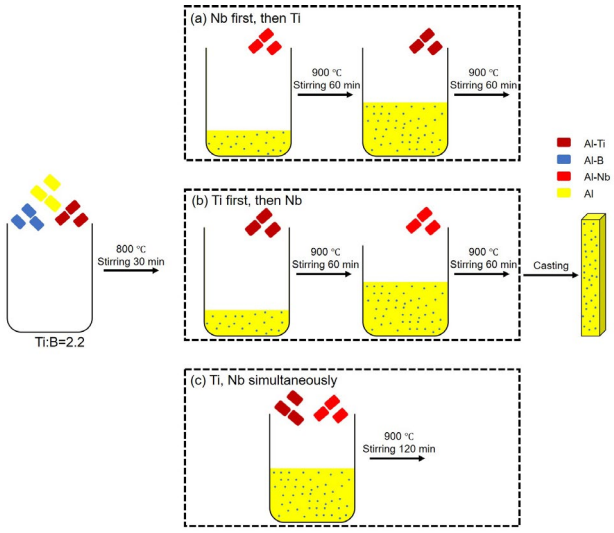

Fig. 1: Schematic diagram of the processing route for introducing Nb and Ti (a–c)

2.2 Grain refinement experiments of Al-4Ti-1Nb-1B master alloys

To comprehensively evaluate the grain refinement performance of Al-4Ti-1Nb-1B prepared with different Nb and Ti introduction sequences, CP-Al and a series of Al-Si alloys (Al-3.5Si, Al-7Si, and Al-10.5Si) were fabricated by melting CP-Al (≥99.9%) with Al-20Si alloys. To modify the eutectic Si phase, 0.2wt.% Al-10Sr was added, followed by the addition of 0.5wt.% Al-4Ti-1Nb-1B grain refiners at 720 °C. The melt was immediately stirred with a graphite rod for 1 min to promote complete melting and uniform dispersion of the grain refiners, and held for 2 min. Then the melt was cast into a Keller-Bühler-Interlaken (KBI) cylindrical steel mold (Φ75 mm×25 mm)[30], which was placed on a refractory brick preheated to 200 °C, as illustrated in Fig. 2. The cooling rate

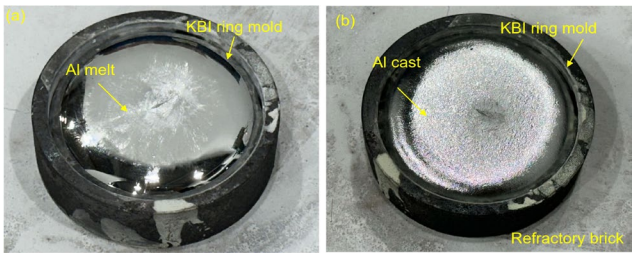

Fig. 2: Keller-Bühler-Interlaken standard solidification experiment: (a) aluminum melt poured into KBI ring mold; (b) solidified aluminum casting

under this solidification condition was approximately 0.4 °C·s^{-1}. For comparison, a commercial Al-5Ti-1B refiner (provided by Advanced Metallurgical Group) was also conducted under same casting conditions to refine the Al-Si alloys.

To accurately determine the grain size of the refined α-Al phase, the surfaces of the aluminum ingots in contact with the refractory brick were ground and polished. An electrolytic corrosion test was conducted using a WY-06 model apparatus, applying an anode coating with a 1wt.% fluoboric acid solution. The α-Al grain size was observed using a polarized optical metallographic microscope (SG-51) and measured by the mean linear intercept method in accordance with ASTM E112-10.

2.3 Characterization of Al-4Ti-1Nb-1B master alloys

Samples were sectioned from Al-4Ti-1Nb-1B. After ground and polished, the microstructure of the Al-4Ti-1Nb-1B was observed using a field emission scanning electron microscope (Phenom-XL G2), and elemental distribution was analyzed via the integrated energy-dispersive X-ray spectroscopy (EDS). To precisely investigate Nb adsorption on the surface of TiB_2 particles, site-specific slices containing representative TiB_2 particles were prepared by focused ion beam (FIB) milling using a Helios G4 CX system. The particle structure and elemental adsorption at nucleation sites were further examined by transmission electron microscopy (Talos F200X). The particle size and aspect ratio of at least 300 TiB_2 particles from each sample were measured using Image Pro Plus.

2.4 First-principles calculations

First-principles calculations based on the density functional theory (DFT) were performed using the Vienna Ab-initio Simulation Package (VASP)[31-35]. Perdew-Burke-Ernzerhof (GGA-PBE) exchange correlation functional was used to calculate the electronic correlation function, and conjugate gradient algorithm was employed to optimize the geometry. The plane-wave cutoff energy of diboride/Al interface system was set to be 450 eV, and the self-consistency convergence criteria for energy tolerance was 10^{-6} eV·atom^{-1}. Relevant interface models were constructed by Materials Studio. To ensure adequate space for all atoms and full relaxation of cells, a vacuum layer of 15 Å was reserved for the surface supercell.

3 Results

3.1 Microstructure of Al-4Ti-1Nb-1B alloys

Figure 3 presents the microstructures of Al-4Ti-1Nb-1B alloys prepared with different Ti and Nb introduction sequences. The alloys primarily contain two secondary phases: MAl_3 (where M presents Ti or Nb) and TiB_2. The constitution and morphology of the MAl_3 phase have been analyzed and discussed in our previous study[36]. Therefore, this work focuses on the characterization and analysis of TiB_2 in different Al-4Ti-1Nb-1B samples. The TiB_2 particles exhibit polyhedral morphology, with some degree of agglomeration observed. EDS mappings confirm the overlapping distribution of Ti and B, indicating the formation of TiB_2. Furthermore, both SEM and EDS analyses reveal that TiB_2 particles in all three

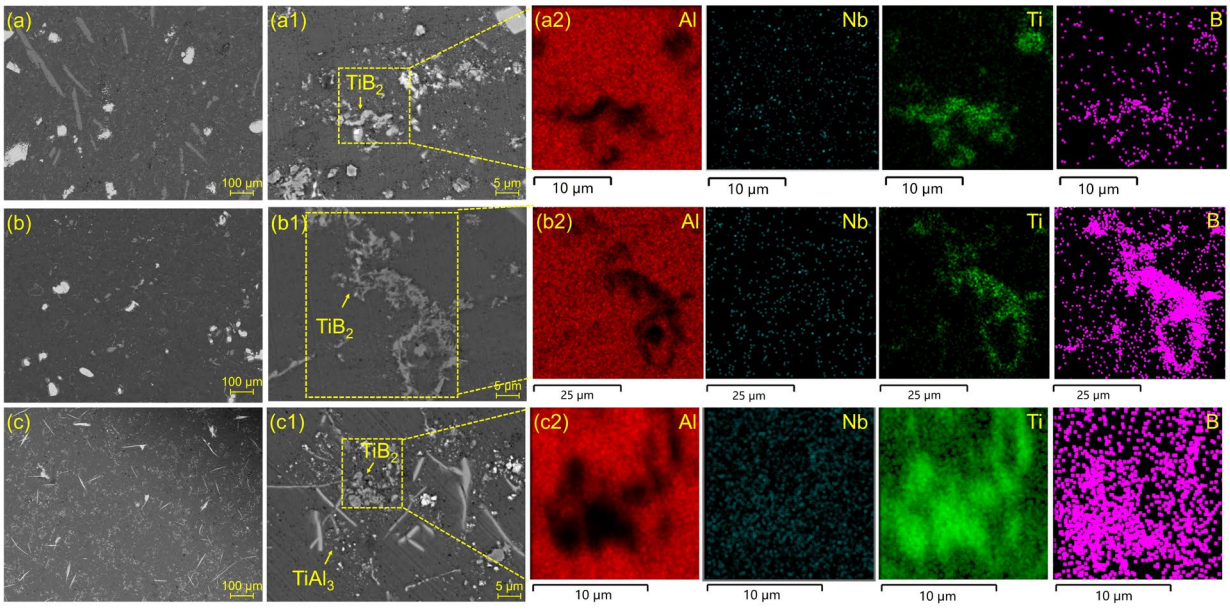

Fig. 3: SEM morphology and EDS maps of TiB_2 phase in Samples A (a, a1–a2), B (b, b1–b2), and C (c, c1–c2)

Al-4Ti-1Nb-1B samples exhibit negligible Nb signals. At this magnification, no evidence of Nb adsorption is observed.

The TiB_2 particle sizes distributions are shown in Fig. 4. For Sample A, the average TiB_2 particle size is 1.02 μm with a standard deviation σ=0.45. The particles are relatively fine and exhibit a uniform distribution. Next, for the Sample B prepared via the Ti-first followed by Nb process, the average TiB_2 particle size is 1.36 μm with σ=0.36. Although slightly larger than the former, the particles remained fine and uniformly distributed. When Nb and Ti are simultaneously introduced, the TiB_2 particles become coarser, with an average size of 1.55 μm and σ=0.41 in Sample C. Comparatively, the stepwise addition of Nb and Ti, either Nb-first or Ti-first, is more effective in controlling the TiB_2 particle size and suppressing the formation of large particles or agglomerates. In contrast, the simultaneous addition of Nb and Ti introduces a higher concentration of Nb and Ti solutes into the melt.

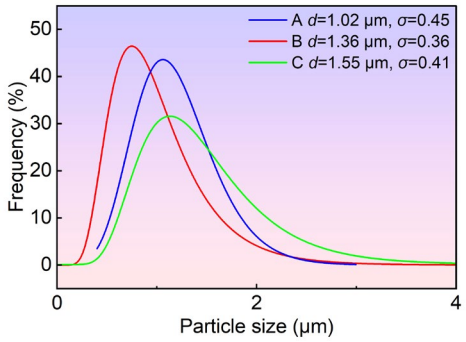

Fig. 4: Statistical results of TiB_2 size (d) in Samples A, B, and C, and standard deviation (σ)

3.2 Grain refinement effect of Al-4Ti-1Nb-1B alloys

Figure 5 presents the grain refinement results of CP-Al, Al-3.5Si, Al-7Si, and Al-10.5Si alloys inoculated with Samples A, B, C, and commercial Al-5Ti-1B. Table 1 summarizes the α-Al grain size after treatment with various refiners, which was used to generate Fig. 6. As shown in Fig. 5, the unrefined alloys (CP-Al, Al-3.5Si, Al-7Si, and Al-10.5Si) exhibit coarse dendritic α-Al grains with an average grain size exceeding 1,500 μm. Among the refiners tested, Sample B acquires the finest grain sizes: 132.3±14.2 μm for CP-Al, 148.5±7.7 μm for Al-3.5Si, 150.1±27.5 μm for Al-7Si, and 311.1±52.2 μm for Al-10.5Si. Sample A exhibits slightly inferior refinement compared to Sample B. Refinement performance of Sample C is intermediate between Samples A and B. Overall, Samples A, B, and C demonstrate superior grain refinement compared to the commercial Al-5Ti-1B refiner.

Fig. 5: Polarized morphologies of α-Al in CP-Al and various Al-Si alloys

Table 1: Average grain sizes (μm) of CP-Al and various Al-Si alloys with different grain refiners

	CP-Al	Al-3.5Si	Al-7Si	Al-10.5Si
Sample A	176.6±7.1	174.8±6.6	207.8±27.1	472.6±8.2
Sample B	132.3±14.2	148.5±7.7	150.1±27.5	311.1±52.2
Sample C	147.5±20.9	152.7±8.2	180.9±13.6	375.6±65.2
Al-5Ti-1B	175.5±28.1	268.7±45.2	541.1±26.3	559.2±46.6
Unrefined	>1,500	>1,500	>1,500	>1,500

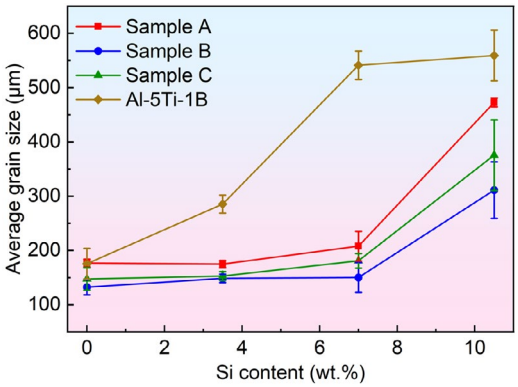

Fig. 6: Grain refinement of Al-Ti-Nb-B with different Si content

Notably, Samples A, B, and C exhibit similarly excellent grain refinement. At higher Si concentrations (7wt.% or 10.5wt.%), Sample B maintains the strongest resistance to Si poisoning and sustained refinement performance. Sample A shows weaker resistance, and Sample C performs intermediate to A and B.

3.3 Nucleation substrates in Al-4Ti-1Nb-1B alloys

To further investigate the factors contributing to the grain refinement performance among Samples A, B, and C, TiB_2 particles from each sample were extracted and thinned using focused ion beam (FIB) techniques. Subsequently, STEM combined with EDS was applied to observe the TiB_2 particles in Samples A, B, and C. Figure 7 summarizes the observations of these particles. Figure 7(a) shows a block-shaped TiB_2 particle from Sample A. The magnified yellow boxed area in Fig. 7(a1) corresponds to the TiB_2/Al interface, where EDS maps confirm a distinct Nb-enriched layer, indicating Nb adsorption. Analysis of the SAED pattern in Fig. 7(b) and the HRTEM image and EDS line scan in Fig. 7(c) reveal that Nb atoms segregate along the $(01\bar{1}0)$ plane on the TiB_2 surface at the TiB_2/Al interface. Figure 7(d) presents a stacked, elongated TiB_2 particle from Sample B. A pronounced Nb-enriched layer is evident on the TiB_2 surface, as shown in Fig. 7(d5). SAED pattern in Fig. 7(e), HRTEM image and EDS line scan in Fig. 7(f) confirm that Nb atoms adsorb along the (0001) plane toward the TiB_2/Al interface. Moreover, Fig. 7(g) depicts a cubic TiB_2 particle from Sample C, with Figs. 7(g1)–(g5) illustrating Nb adsorption on its surface. The Nb distribution at the TiB_2/Al interface in Sample C is further detailed in Figs. 7(g) and (h).

In summary, all TiB_2 particles from Samples A, B, and C exhibit evident Nb adsorption on the TiB_2/Al interface. Comparative EDS line scans of Nb along the TiB_2/Al interfaces in Figs. 7(c), (f), and (i) indicate that Sample B exhibits the most pronounced Nb adsorption with the highest Nb concentration, followed by Sample C and then Sample A. Correspondingly, Sample B demonstrates superior grain refinement performance across CP-Al, Al-3.5Si, Al-7Si, and Al-10.5Si alloys, especially at higher Si contents (Al-7Si and Al-10.5Si), compared to Samples A and C. Therefore, subsequent analyses focus on the influence of Nb adsorption on the TiB_2 surface on its grain refinement performance.

4 Discussion

4.1 Effect of Ti and Nb introduction sequence on Nb adsorption on the TiB_2 surface

In the above experimental investigations, the TiB_2 particles in Sample B prepared by introducing Ti prior to Nb, exhibit the most pronounced Nb surface adsorption. This is considered a major factor contributing to the superior grain refinement performance of Sample B in CP-Al, Al-3.5Si, Al-7Si, and Al-10.5Si alloys. To elucidate the mechanism behind this observation, TiB_2/Al interface models with different Ti and Nb addition sequences are constructed to investigate their influence on Nb adsorption behavior on the TiB_2 surface.

According to the process shown in Fig. 1(b), during the 60 min holding period at 900 °C after the addition of the Al-Ti alloy, the melt contains insoluble TiB_2 particles and excess Ti and Al. This condition resembles that used in the preparation of Al-Ti-B grain refiners. Based on the work by Fan et al.[37, 38], such an environment facilitates the formation of a two-dimensional $TiAl_3$ compound ($TiAl_3$ 2DC) on the (0001) surface of TiB_2. Following this, Nb is introduced. Nb atoms diffuse through the pre-formed $TiAl_3$ 2DC layer and incorporate into the interface, leading to the formation of a reconstructed Nb adsorbed layer structure. The presence of the $TiAl_3$ 2DC layer partially provides a thermodynamic driving force for Nb atoms to occupy the remaining active sites, thereby producing a lower-energy, more stable interfacial configuration. Our previous study confirmed that in the presence of excess Nb in the melt, a $NbAl_3$ 2DC layer can form at the TiB_2 surface[29]. Figures 8(a1)–(a3) illustrate this evolution process. TiB_2 initially coated with a $TiAl_3$ 2DC layer undergoes Nb diffusion into the 2DC, forming $NbAl_3$ 2DC, followed by further Nb diffusion into the TiB_2 particles, ultimately producing Nb surface adsorption. This process reflects a balance of kinetic diffusion of Nb atoms and the thermodynamic preference for low-energy interface formation, which together favor the creation of highly active and stable nucleation sites.

In contrast, when TiB_2 is synthesized in situ prior to Ti and Nb addition, as shown in Fig. 1(a), the Ti/B ratio is controlled at 2.2, and the reaction is maintained for 30 min. Under this condition, no excess Ti remains to form a $TiAl_3$ 2DC layer.The

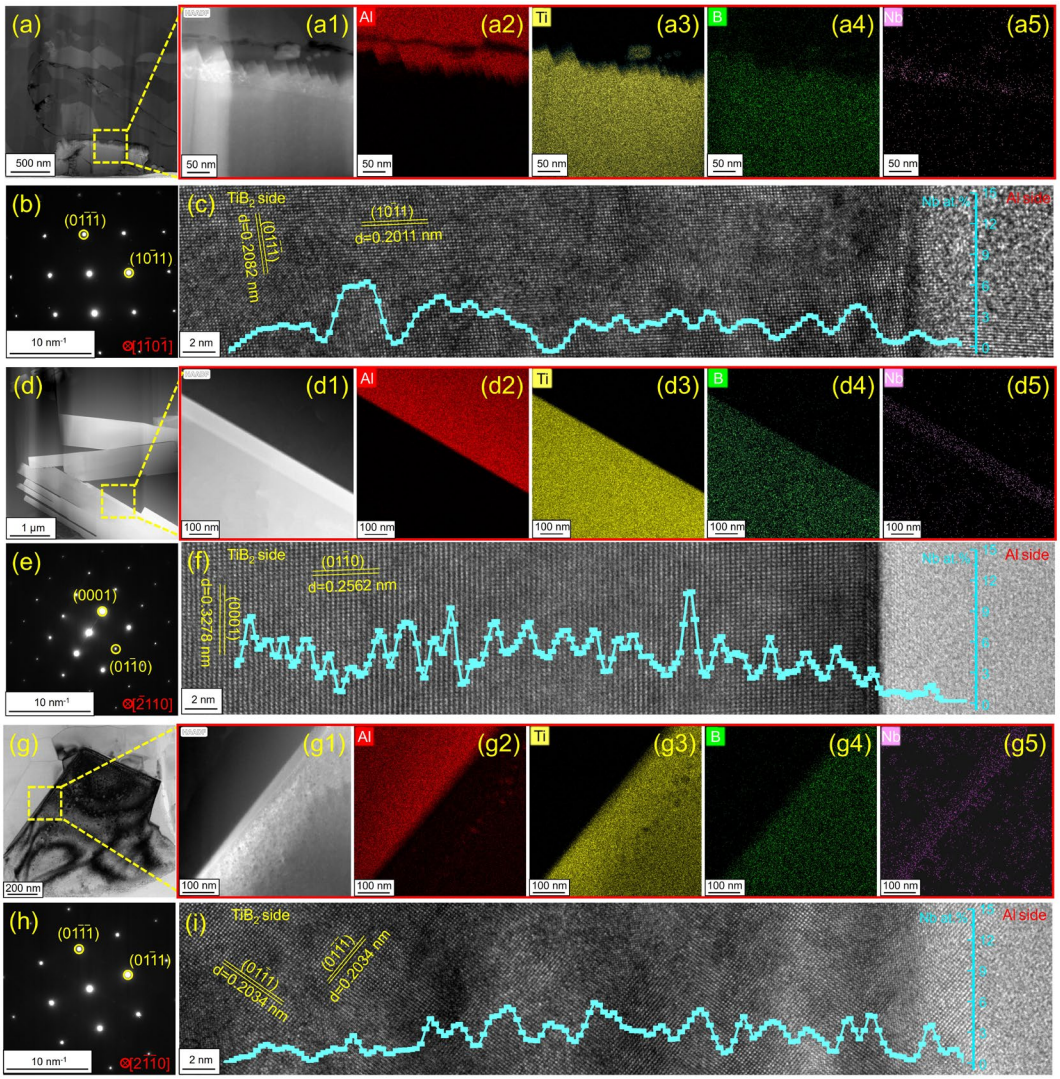

Fig. 7: TiB_2 particle in Sample A and corresponding EDS maps (a, a1–a5), SAED pattern of the yellow box in (a) (b), HRTEM image of the surface of TiB_2 in Sample A and the EDS line-scanning pattern of Nb (c), TiB_2 particle in Sample B and corresponding EDS maps (d, d1–d5), SAED pattern of the yellow box in (d) (e), HRTEM image of the surface of TiB_2 in Sample B and the EDS line-scanning pattern of Nb (f), TiB_2 particle in Sample C and corresponding EDS maps (g, g1–g5), SAED pattern of the yellow box in (g) (h), and HRTEM image of the surface of TiB_2 in Sample C and the EDS line-scanning pattern of Nb (i)

absence of this pre-formed $TiAl_3$ 2DC leads to a higher-energy Nb adsorption structure. Although Nb still adsorbs, the resulting interface lacks the structural ordering and low-energy stabilization provided by the Ti-first sequence. Consequently, the Ti-first addition promotes the formation of a lower-energy, well-ordered Nb adsorbed interface, which maximizes the stability of interfacial sites and enhances heterogeneous nucleation efficiency. Figures 8(b1)–(b3) illustrate the interface evolution under the Nb-first route. The ground-state energies for both addition sequences were calculated using the ab initio method and summarized in Fig. 8(c). It is evident that the Ti-first followed by Nb introduction sequence provides a smaller ground-state energy change (ΔE), lower intermediate energy levels, and a stronger thermodynamic driving force, whereas the Nb-first route favors more continuous Nb surface coverage. Consequently, Sample B exhibits the most pronounced Nb adsorption on the TiB_2 surface, followed by Sample C, while Sample A shows the weakest adsorption. These differences in Nb adsorption and interface structure explain how the addition sequence controls both the stability and distribution of active nucleation sites, which directly impacts grain refinement behavior in Al alloys.

4.2 Effect of Nb adsorption amount on grain refinement performance and Si-poisoning resistance

The grain refinement results shown in Fig. 5 demonstrate that Sample B exhibits superior refinement efficiency for CP-Al, Al-3.5Si, Al-7Si, and Al-10.5Si compared to Samples A and C. The Nb elemental line scans presented in Figs. 7(c), (f), and (i) reveal significant differences in Nb adsorption at the TiB_2 surfaces among the three samples. The corresponding Nb line scan profiles for Samples A, B, and C are compared in Fig. 9, with their average and maximum Nb concentrations summarized in Table 2. Sample B shows the highest Nb surface adsorption on TiB_2, with an average

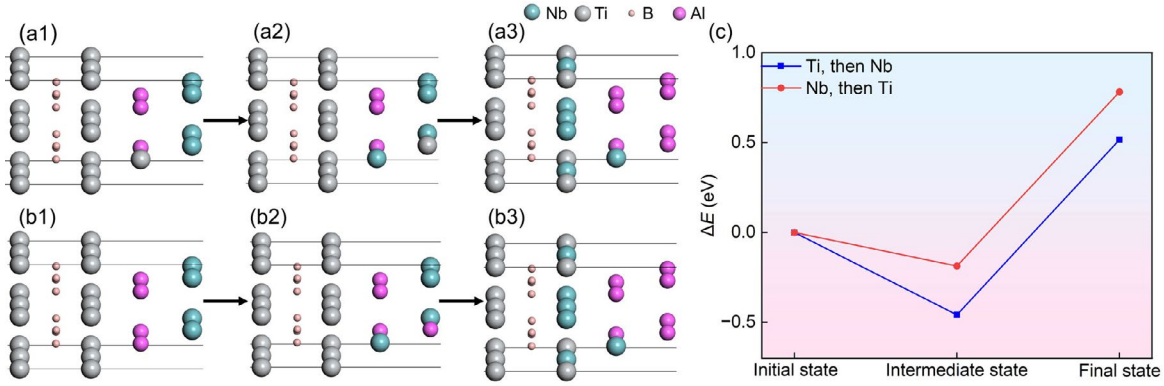

Fig. 8: Reconstruction of the TiB_2/Al interface under the introduction sequence of Ti followed by Nb (a1–a3), reconstruction of the TiB_2/Al interface under the introduction sequence of Nb followed by Ti (b1–b3), and energy variation, Δ*E*, induced by the introduction sequence of Ti and Nb (c)

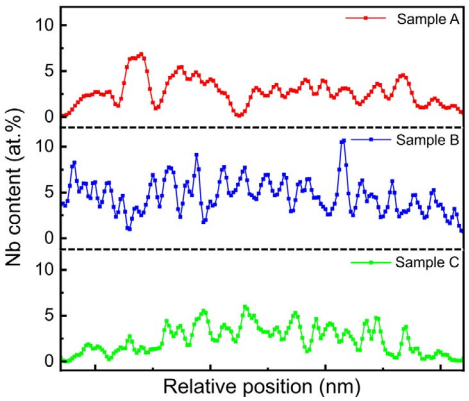

Fig. 9: EDS line-scanning patterns showing the composition profiles of Nb on the surface of TiB_2

Table 2: Nb content on the surface of TiB_2 in Al-4Ti-1Nb-1B

Grain refiner	Average Nb content (at.%)	Maximum Nb content (at.%)
Sample A	2.03	6.85
Sample B	3.80	10.68
Sample C	2.38	5.98

Nb content of 3.80at.%, which significantly exceeds the critical threshold of 1.92at.% previously reported to activate TiB_2 as an effective nucleation site[36]. Sample C exhibits a moderate Nb adsorption level of 2.38at.%, while Sample A presents the lowest, at only 2.03at.%. Although all three samples outperform the commercial Al-5Ti-1B refiner in refining CP-Al and various Al-Si alloys, the grain refinement performance of Sample B is clearly superior to that of Sample C, and markedly better than that of Sample A. Therefore, the influence of Nb adsorption content on the TiB_2 surface on grain refinement and Si-poisoning resistance was investigated in detail.

To quantify the nucleation tendency of α-Al on the TiB_2 surface, the adhesion energy W_{ad}, which represents the work required to separate one interface into two free surfaces, was calculated using the following equations[39, 40]:

$$W_{ad} = \frac{1}{A}(E_{slab}^{Al} + E_{slab}^{TiB_2} - E_{interface}) \quad (1)$$

where $E_{interface}$, E_{slab}^{Al}, and $E_{slab}^{TiB_2}$ were calculated by the *ab initio* method, denoting the ground state energies of the interface model, the Al, and the substrate slab, respectively. W_{ad} denotes the adhesion energy of the TiB_2/Al and interface, and A denotes the interfacial area of the TiB_2/Al interface. Various TiB_2/Al interfaces incorporating different numbers of Nb atoms are constructed, as shown in Fig. 10. For comparison, the TiB_2/Al interface from commercial Al-5Ti-1B was also modeled, based on previous studies[37, 41, 42]. The adhesion energies, W_{ad}, of the corresponding interface models are calculated and presented in Fig. 10(b). The adhesion energy of the TiB_2/Al interface without Nb atoms is 3.72 $J \cdot m^{-2}$, which is in good agreement with the result reported by Li et al (3.77 $J \cdot m^{-2}$)[25]. For comparison, the W_{ad} of the TiB_2/Al interface with one Nb atom increases to 3.93 $J \cdot m^{-2}$. With the adsorption of two Nb atoms, W_{ad} increases to 3.96 $J \cdot m^{-2}$. The adhesion energies of TiB_2/Al interfaces with three and four Nb atoms are 3.97 and 3.95 $J \cdot m^{-2}$, respectively. These results demonstrate that Nb adsorption significantly increases the adhesion energy of the TiB_2/Al interface, forming a more thermodynamically stable structure. Importantly, the Ti-first addition sequence promotes the formation of a low-energy, well-ordered Nb adsorbed interface. In contrast, Nb-first addition produces a higher-energy interface with less ordered Nb adsorption. The lower-energy Ti-first interface stabilizes heterogeneous nucleation sites more effectively, which promotes more uniform nucleation of α-Al grains.

Thus, the Nb adsorption at the TiB_2 surface is the key factor contributing to the superior grain refinement performance of Samples A, B, and C. Overall, these findings indicate that both the amount and spatial distribution of Nb at the TiB_2/Al interface, determined by the addition sequence, critically affect the effectiveness of Al-Ti-Nb-B refiners. Ti-first addition produces the most favorable, low-energy interfacial structure, which maximizes grain refinement efficiency.

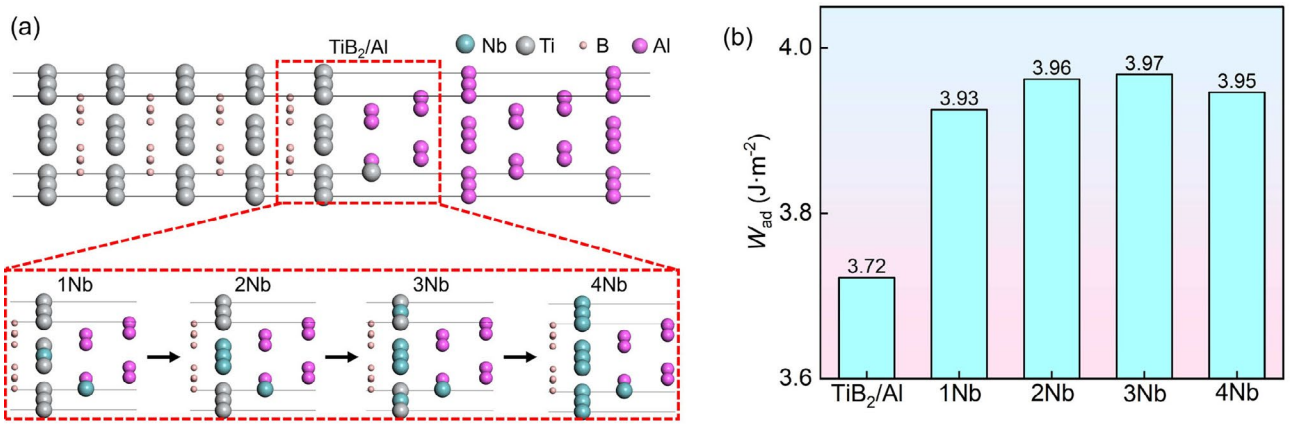

Fig. 10: Effect of Nb adsorption on TiB_2/Al interface on adhesion energy W_{ad}: (a) TiB_2/Al interface models with various Nb atoms; (b) variation of adhesion energy W_{ad} of corresponding structures

In addition, the superior resistance to Si poisoning of Sample B is a critical distinguishing feature, compared to Samples A and C. It is important to investigate the influence of Nb adsorption on Si atoms at the TiB_2 surface. To quantitatively compare the Si adsorption propensity at TiB_2/Al and TiB_2(Nb)/Al interfaces, the Si adsorption factor $\kappa_{Si}(c_{Si})$ is defined[25]

$$\kappa_{Si}(c_{Si}) = \frac{W_{ad(c_{si})}}{W_{ad(0)}} \quad (2)$$

where $W_{ad(c_{Si})}$ and $W_{ad(0)}$ denote the adhesion energies when the Si concentration at the interface is c_{Si} and 0, respectively. The TiB_2/Al interfaces with adsorbed Si atoms and their corresponding segregation tendency, denoted as $\kappa_{Si}(c_{Si})$, are presented in Fig. 11. As the interfacial Si concentration (c_{Si}) increases from 0.00 to 1.00, $\kappa_{Si}(c_{Si})$ of both TiB_2/Al and TiB_2/Al with 1 Nb rises, indicating a higher tendency for Si segregation at higher concentrations. When the interfacial Si concentration (c_{Si}) increases from 0.75 to 1.00, the $\kappa_{Si}(c_{Si})$ of TiB_2/Al with 2, 3 or 4 Nb no longer increases. This trend reflects the natural thermodynamic driving force for Si atoms to accumulate at the interface, which can potentially poison the nucleation sites of α-Al. However, $\kappa_{Si}(c_{Si})$ is lower for TiB_2/Al interfaces with 2 Nb atoms than with 1 Nb, and both are lower than the Nb-free interface, suggesting that greater Nb segregation reduces Si accumulation. This implies that the presence of Nb at the interface effectively competes with Si for adsorption sites, thereby mitigating the adverse effects of Si on nucleation efficiency. For TiB_2/Al interfaces with 3 or 4 Nb atoms, $\kappa_{Si}(c_{Si})$ reaches a maximum at c_{Si}=0.75 and then decreases as c_{Si} increases to 1, indicating that further Si enrichment becomes increasingly difficult at higher Nb concentrations. Furthermore, $\kappa_{Si}(c_{Si})$ consistently decreases with increasing Nb content from 1 to 4 Nb atoms under the same c_{Si}, reinforcing the conclusion that higher Nb adsorption at the TiB_2/Al interface suppresses Si segregation. Collectively, these results provide a clear atomic-scale explanation for the improved resistance to Si poisoning observed in Nb-enriched grain refiners. These findings explain why Sample B, which exhibits the highest Nb adsorption content at the TiB_2 surface, achieves superior refinement performance in Al-7Si and Al-10.5Si alloys compared to Samples A and C.

In summary, the enhanced grain refinement and Si-poisoning resistance in Sample B can be attributed to the higher Nb adsorption on the TiB_2 surface. As shown in Fig. 12, Ti is first introduced to form a Ti-rich Al-Ti-B melt. Nb is then added, and through substitution of Ti in the $TiAl_3$ 2DC layer and

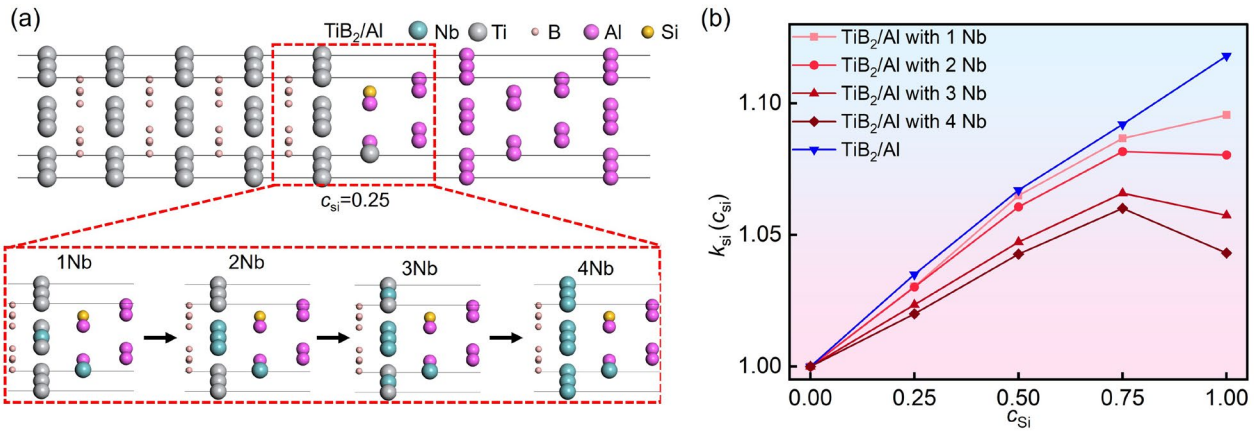

Fig. 11: Effect of Nb adsorption at TiB_2/Al interface on Si segregation propensity, $\kappa_{Si}(c_{Si})$: (a) TiB_2/Al interfaces with various Nb atoms and Si segregation; (b) variation of $\kappa_{Si}(c_{Si})$ for corresponding interfaces

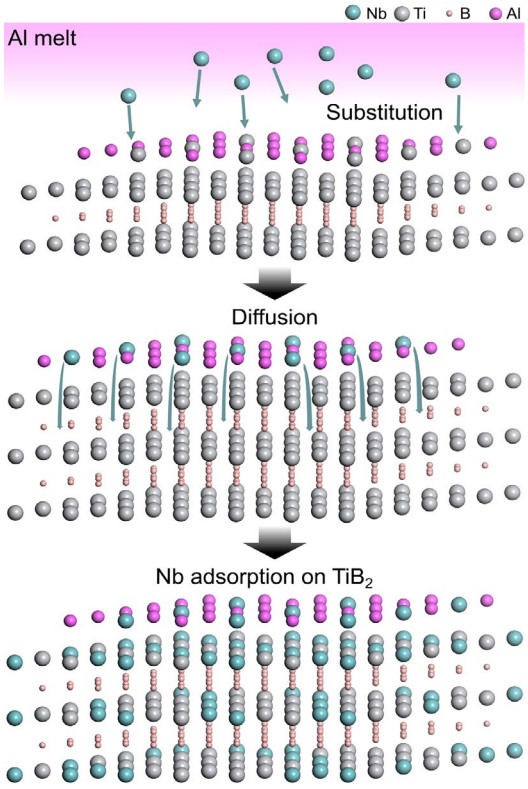

Fig. 12: A schematic illustration of the Nb adsorption mechanisms on TiB_2

subsequent diffusion, Nb atoms are incorporated into the TiB_2 surface, leading to a significant content of Nb adsorption. This unique Nb adsorption increases the interfacial adhesion energy W_{ad} and reduces the Si segregation tendency $\kappa_{Si}(c_{Si})$ at the TiB_2/Al interface. The higher the Nb content at the interface, the stronger the resistance to Si poisoning. The superior performance of Sample B is thus attributed to an average Nb content of 3.80at.%, which optimizes both grain refinement and resistance to Si poisoning.

5 Conclusions

In this study, a series of Al-4Ti-1Nb-1B grain refiners were prepared via different sequences for introducing Ti and Nb. It was found that the sequence of Ti and Nb addition significantly influences the adsorption behavior of Nb on the TiB_2 surface, thereby affecting both the grain refinement efficiency and resistance to Si poisoning. The following conclusions can be drawn:

(1) All Al-4Ti-1Nb-1B refiners, regardless of the Ti and Nb addition sequence, exhibit excellent grain refinement performance in low-Si aluminum alloys such as CP-Al and Al-3.5Si. For high-Si alloys such as Al-7Si and Al-10.5Si, the refiner synthesized by first adding Ti followed by Nb demonstrates the best refinement performance, refining the α-Al grain size of Al-7Si to 150.1±27.5 μm.

(2) Introducing Ti prior to Nb leads to the most pronounced Nb adsorption on the TiB_2 surface. Initially, Ti promotes the formation of a $TiAl_3$ 2DC on the in-situ formed TiB_2. Subsequently, due to thermodynamic driving forces favoring lower ground-state energy, Nb atoms replace Ti in the surface $TiAl_3$ 2DC and gradually diffuse into the TiB_2, forming a stable Nb-enriched layer. The ground-state energy change ΔE for the Ti prior to Nb process is lower than that of the reverse sequence, making Nb adsorption more favorable in this route.

(3) Varying degrees of Nb adsorption are observed on the TiB_2 surface. The highest concentration, 3.80at.%, is obtained in the sample introducing Ti prior to Nb. First-principles calculations reveal that higher Nb content enhances the TiB_2/Al interfacial adhesion energy W_{ad} and suppresses the segregation tendency of Si atoms, represented by $\kappa_{Si}(c_{Si})$. The Nb adsorption on the TiB_2 surface is thus the key factor contributing to the superior performance of the Al-4Ti-1Nb-1B refiners. A higher level of Nb adsorption on the TiB_2 surface leads to improved refinement performance and stronger Si-poisoning resistance, particularly in high-Si alloys such as Al-7Si and Al-10.5Si.

Acknowledgments

The authors gratefully acknowledge the financial support by the Fundamental Research Funds for the Central Universities (Grant Nos. YWF-22-L-1284, YWF-23-Q-1097).

Conflict of interest

The authors declare that they have no conflict of interest.

References

[1] Easton M A, Qian M, Prasad A, et al. Recent advances in grain refinement of light metals and alloys. Current Opinion in Solid State & Materials Science, 2016, 20(1): 13–24.
[2] Feng W, Yulung C, Dmitry E, et al. A grain refinement mechanism of cast commercial purity aluminium by vanadium. Materials Characterization, 2021, 181: 111468.
[3] ASM Handbook, Volume 15: Casting, ASM International 2008.
[4] Stjohn D H, Easton M A, Qian M, et al. Grain refinement of magnesium alloys: A review of recent research, theoretical developments and their application. Metallurgical and Materials Transactions: A, 2013, 44(7): 2935–2949.
[5] Robles F, Hernandez J, and Ramirez R M. Al-Si alloys: Automotive, aeronautical, and aerospace applications. Springer International Publishing AG, 2017.
[6] Murty B, Kori S, and Chakraborty M. Grain refinement of aluminium and its alloys by heterogeneous nucleation and alloying. Metallurgical Reviews, 2002, 47(1): 3–29.
[7] Jones G P. New ideas on the mechanism of heterogeneous nucleation in liquid aluminium. National Physical Laboratory Division of Chemical Standards, Teddington, UK, 1980.
[8] Greer A, Bunn A, Tronche A, et al. Modelling of inoculation of metallic melts: Application to grain refinement of aluminium by Al-Ti-B. Acta Materialia, 2000, 48(11): 2823–2835.
[9] Li Y, Hu B H, Liu B, et al. Insight into Si poisoning on grain refinement of Al-Si/Al-5Ti-B system. Acta Materialia, 2020, 187: 51–65.
[10] Birol Y. Effect of silicon content in grain refining hypoeutectic Al-Si foundry alloys with boron and titanium additions. Materials Science & Technology, 2014, 28(4): 385–389.

[11] Quested T, Dinsdale A, Greer A, et al. Thermodynamic evidence for a poisoning mechanism in the Al-Si-Ti system. Metal Science Journal, 2013, 22(9): 1126–1134.
[12] Wang Y, Que Z, Hashimoto T, et al. Mechanism for Si poisoning of Al-Ti-B grain refiners in Al alloys. Metallurgical and Materials Transactions: A, 2020, 51(11): 5743–5757.
[13] Bolzoni L, Babu N. Refinement of the grain size of the LM25 alloy (A356) by 96Al-2Nb-2B master alloy. Journal of Materials Processing Technology, 2015, 222: 219–223.
[14] Bolzoni L, Nowak M, Babu N. Grain refinement of Al-Si alloys by Nb-B inoculation. Part II: Application to commercial alloys. Materials & Design, 2015, 66: 376–383.
[15] Bolzoni L, Nowak M, Babu N. Assessment of the influence of Al-2Nb-2B master alloy on the grain refinement and properties of LM6 (A413) alloy. Materials Science and Engineering: A, 2015, 628(25): 230–237.
[16] Li Y, Jiang Y, Liu B, et al. Understanding grain refining and anti Si-poisoning effect in Al-10Si/Al-5Nb-B system. Journal of Materials Science & Technology, 2021, 65: 190–201.
[17] Zhao J, Jackeson M, and Peluso L. Mapping of the Nb-Ti-Si phase diagram using diffusion multiples. Materials Science and Engineering: A, 2004.
[18] Li Y, Hu B H, Gu Q, et al. Achievement in grain-refining hypoeutectic Al-Si alloys with Nb. Scripta Materialia, 2019, 160: 75–80.
[19] Xu J, Li R, Li Q, et al. Effect of agglomeration on nucleation potency of inoculant particles in the Al-Nb-B master alloy: Modeling and experiments. Metallurgical and Materials Transactions: A, 2021, 52(3): 1077–1094.
[20] Xu J, Li Y, Hu B H,et al. Development of Al-Nb-B master alloy with high Nb/B ratio for grain refinement of hypoeutectic Al-Si cast alloys. Journal of Materials Science, 2019, 54(23): 14561–14576.
[21] Xu J, Li Y, Ma K, et al. In-situ observation of grain refinement dynamics of hypoeutectic Al-Si alloy inoculated by Al-Ti-Nb-B alloy. Scripta Materialia, 2020, 187: 142–147.
[22] Li Y, Jiang Y, Hu B H, et al. Novel Al-Ti-Nb-B grain refiners with superior efficiency for Al-Si alloys. Scripta Materialia, 2020, 187(1): 262–267.
[23] Zhu L, Zhang Y, Li Q, et al. Effectively refining Al-10Si alloy via Al-Ti-Nb-B refiner with Nb_2O_5. Journal of Materials Science & Technology, 2024, 176(9): 204–210.
[24] Wu D Y, Ma S D, Jing T, et al. Revealing the mechanism of grain refinement and anti Si-poisoning induced by (Nb, Ti)B_2 with a sandwich-like structure. Acta Materialia, 2021, 219: 117265.
[25] Li D X, Yan X, Fan Y, et al. An anti Si/Zr-poisoning strategy of Al grain refinement by the evolving effect of doped complex. Acta Materialia, 2023, 249: 118812.
[26] Li D X, Zhao K, Liu X F, et al. Revealing the correlation of microstructure configuration and mechanical properties of Al-Si-Mg alloy reinforced by C-doped TiB_2 and SiC. Materials Design, 2023, 226: 111694.
[27] Li D X, Zhao K, Han M, et al. Optimizing microstructure and enhancing mechanical properties of Al-Si-Mg-Mn-based alloy by novel C-doped TiB_2 particles. Journal of Materials Research and Technology, 2023, 26: 17.
[28] Xue L W, Jia H, Ma P, et al. Influence of V/B ratio and rolling treatment on the grain refinement efficacy and anti-fading ability of Al-V-B master alloys. Materials Characterization, 2025, 219: 114596.
[29] Yi H, Cheng Y, Zhang H R, et al. Simultaneous integration of anti Si-poisoning and anti-fading properties on an innovative Al grain refiner via Nb-modified TiB_2. Journal of Alloys and Compounds, 2024, 995: 174707.
[30] Trujillo and Javier F. A strict formulation of a nonlinear Helmholtz equation for the propagation of sound in bubbly liquids. Part I: Theory and validation at low acoustic pressure amplitudes. Ultrasonics Sonochemistry, 2018, 47: 75–98.
[31] Blochl P E. Projector augmented-wave method. Physical Review: B, 1994, 50: 17953–17979.
[32] Kresse G, Hafner K. Ab initio molecular-dynamics simulation of the liquid-metal-amorphous-semiconductor transition in germanium. Physical Review: B, 1994, 49: 14251.
[33] Kresse G and Furthmuller J. Efficient iterative schemes for ab initio total-energy calculations using a plane-wave basis set. Physical Review: B, 1996, 54: 11169–11186.
[34] Perdew J, Burke K, and Ernzerhof M. Generalized gradient approximation made simple. Physical Review Letters, 1998, 77(18): 3865–3868.
[35] Kresse G and Joubert D. From ultrasoft pseudopotentials to the projector augmented-wave method. Physical Review: B, 1999, 59: 1758–1775.
[36] Yi H, Cheng Y, Zhang H R, et al. Nb adsorption effect and mechanism on Al/TiB_2 interface in novel low-Nb Al-Ti-Nb-B grain refiner. Applied Surface Science, 2025, 710: 164005.
[37] Fan Z, Wang Y, Zhang Y, et al. Grain refining mechanism in the Al/Al-Ti-B system. Acta Materialia, 2015, 84: 292–304.
[38] Men H, and Fan Z. Effects of solute content on grain refinement in an isothermal melt. Acta Materialia, 2011, 59: 2704–2712.
[39] Liu L. First-principles study of polar Al/TiN(111) interfaces. Acta Materialia, 2004, 52(12): 3681–3688.
[40] Siegel D J, Hector L, and Adams J. First-principles study of metal-carbide/nitride adhesion: Al/VC vs. Al/VN. Acta Materialia, 2002, 50(3): 619–631.
[41] Men H and Fan Z. Atomic ordering in liquid aluminium induced by substrates with misfits. Computational Materials Science, 2014, 85: 1–7.
[42] Fan Z, Wang Y, Xia M, et al. Enhanced heterogeneous nucleation in AZ91D alloy by intensive melt shearing. Acta Materialia, 2009, 57(16): 4891–4901.